Journal of Medicinal Chemistry

Article

pubs.acs.org/jmc

Design, Synthesis, and Evaluation of Thyronamine Analogues as Novel Potent Mouse Trace Amine Associated Receptor 1 (*m*TAAR1) Agonists

Grazia Chiellini,*[,†] Giulia Nesi,[‡] Maria Digiacomo,[‡] Rossella Malvasi,[‡] Stefano Espinoza,[§] Martina Sabatini,[†] Sabina Frascarelli,[†] Annunziatina Laurino,[∥] Elena Cichero,[⊥] Marco Macchia,[‡] Raul R. Gainetdinov,[#,¶] Paola Fossa,[⊥] Laura Raimondi,[∥] Riccardo Zucchi,[†] and Simona Rapposelli*[,‡]

[†]Department of Pathology, University of Pisa, 56100 Pisa, Italy

[‡]Deptartment of Pharmacy, University of Pisa, via Bonanno 6, 56100 Pisa, Italy

[§]Department of Neuroscience and Brain Technologies, Istituto Italiano di Tecnologia, 16163 Genova, Italy

[∥]Department of NEUROFARBA, Section of Pharmacology, University of Florence, 50121 Firenze, Italy

[⊥]Department of Pharmacy, University of Genoa, 16126 Genoa, Italy

[#]Institute of Translational Biomedicine, St. Petersburg State University, St. Petersburg, 199034, Russia

[¶]Skolkovo Institute of Science and Technology (Skoltech), Skolkovo, Moscow region, 143025, Russia

S *Supporting Information*

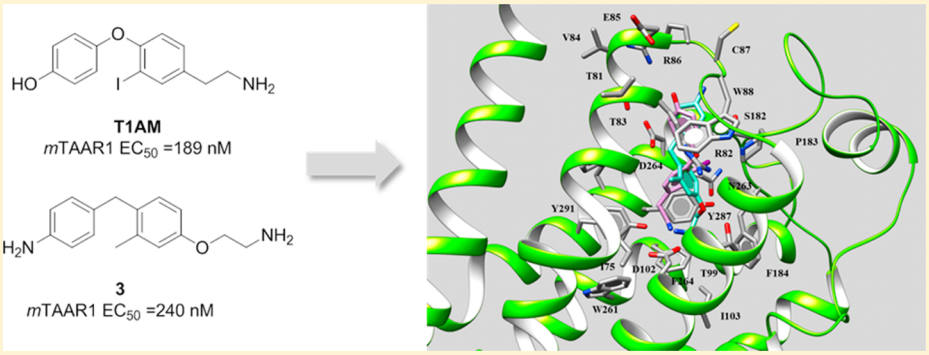

ABSTRACT: Trace amine associated receptor 1 (TAAR1) is a G protein coupled receptor (GPCR) expressed in brain and periphery activated by a wide spectrum of agonists that include, but are not limited to, trace amines (TAs), amphetamine-like psychostimulants, and endogenous thyronamines such as thyronamine (T0AM) and 3-iodothyronamine (T1AM). Such polypharmacology has made it challenging to understand the role and the biology of TAAR1. In an effort to understand the molecular basis of TAAR1 activation, we rationally designed and synthesized a small family of thyronamine derivatives. Among them, compounds **2** and **3** appeared to be a good mimic of the parent endogenous thyronamine, T0AM and T1AM, respectively, both in vitro and in vivo. Thus, these compounds offer suitable tools for studying the physiological roles of mouse TAAR1 and could represent the starting point for the development of more potent and selective TAAR1 ligands.

INTRODUCTION

Thyronamines (TAMs) are naturally occurring signaling compounds, originally postulated to derive from thyroid hormone (T4) throughout deiodination and decarboxylation.[1] Although these compounds were first described almost seven decades ago, their importance was not recognized until 2004, when Scanlan's group identified them as potential ligands of the trace amine associated receptor 1 (TAAR1).[1] So far, two representatives of TAMs, namely 3-iodothyronamine (T1AM) and thyronamine (T0AM) (Figure 1), have been detected in vivo, with T1AM being the most abundant.[1,2]

T1AM has been detected in human blood and virtually in every tissue in rodents at concentrations on the order of a few pmol/g. The pathway responsible for T1AM biosynthesis is still unclear. In human patients subjected to thyroidectomy and undergoing replacement therapy with oral thyroxine, plasma T1AM levels were reported to be normal, suggesting peripheral conversion of T4 to T1AM.[3] However, T1AM decreased in rat liver after treatment with perchlorate and methimazole, but liver concentration was not normalized after ip treatment with exogenous T4, suggesting that T1AM is produced by the thyroid gland and is not an extra-thyroidal metabolite of T4.[4] A

Received: April 2, 2015
Published: May 26, 2015

DOI: 10.1021/acs.jmedchem.5b00526
J. Med. Chem. 2015, 58, 5096−5107

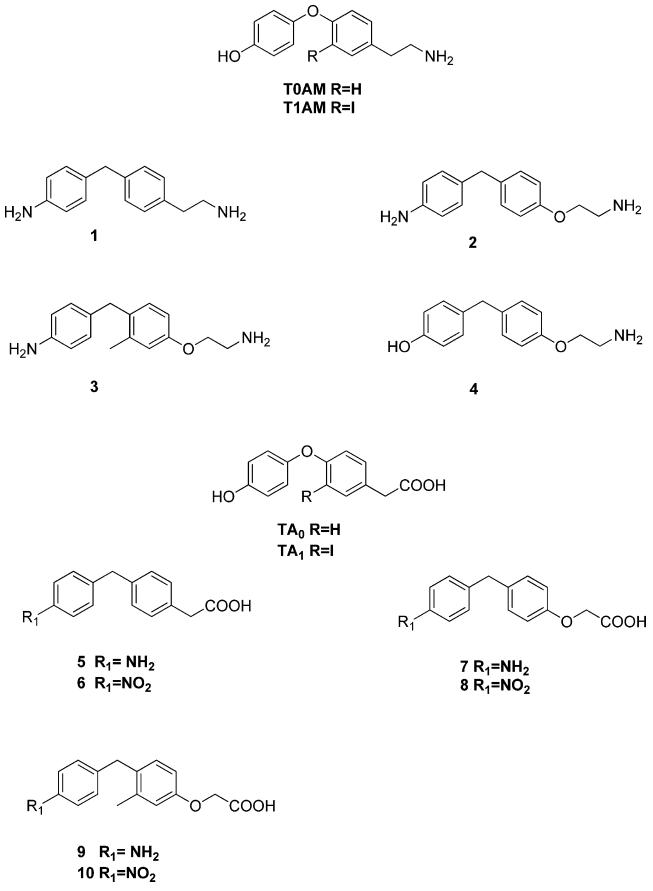

Figure 1. Structures of endogenous thyronamines and new synthetic analogues.

preliminary evidence on the T4 conversion into T1AM on an everted gut sac model has been recently reported.[5]

T1AM should be regarded as a chemical messenger because it interacts with specific receptors and produces significant functional effects. T1AM is not a ligand for nuclear thyroid hormone receptors (TRs), instead it stimulates with nanomolar affinity TAAR1, which is the best characterized TAAR member, found in specific areas of the central nervous system as well as in certain peripheral tissues.[6−10] Recent evidence gained by using transgenic animals and newly developed pharmacological tools indicates that targeting TAAR1 may provide new therapeutic approach for a range of neuropsychiatric and metabolic disorders[6] T1AM binding to TAAR1 engages $G\alpha_s$-type G proteins that activate adenylyl cyclases,[1] but notably, this compound also interacts with amine transporters, with mitochondrial proteins, and binds with high affinity to apoB100.[11] Recently, an inverse agonistic action at TAAR5 has also been described.[12] Administration of exogenous T1AM to rodents caused transient decrease in body temperature and reduction of cardiac inotropic and chronotropic state.[1,13,14] While these effects occurred at micromolar concentration, metabolic and neurological effects were observed at lower dosages, which increased endogenous tissue concentration by about 1 order of magnitude.[15]

T1AM favors fatty acid oxidation over carbohydrate oxidation,[16,17] and chronic treatment with exogenous T1AM in obese mice produced a significant reduction in body weight in the absence of changes in food consumption.[17] T1AM has also been reported to have neuromodulatory effects because icv administration in mice elicited pro-learning and antiamnestic effects.[18] Intracerebral injection also produced hormonal changes, i.e., stimulation of glucagon and inhibition of insulin secretion[19−21] and modifications of alimentary behavior.[22] Although its physiological function remains elusive, T1AM has already revealed promising therapeutic potential. It is noteworthy that the structural similarities between thyroxine, T1AM, and monoamine neurotransmitters suggest an intriguing role for T1AM as both a neuromodulator and a hormone-like molecule that may constitute a part of thyroid hormone action.

All these findings convey that this molecule may have great potential for a wide variety of therapeutic applications, such as obesity, weight loss, neuropsychiatric disorders, and cancer. Unfortunately, thyronamines are rapidly metabolized by different enzyme systems such as amino-oxidase (MAO, SSAO), deiodinases (DIO3), sulfotransferases (SULT1A1 and SULT1A3), *N*-acetyltransferases, and glucuronidases[23,24] and that can obviously constitute a limit to their therapeutic use.

Consequently, the great therapeutic potential as well as the lack of new tools to elucidate T1AM physiological function urge the development of novel synthetic analogues of T1AM.

Herein, we describe the synthesis and properties of a small series (**1**−**10**) of new synthetic analogues of thyronamines (Figure 1). These compounds were screened in vitro for TAAR1 activation, and selected compounds were evaluated in vivo to characterize their functional and metabolic effects. Furthermore, to rationalize the pharmacological results and to support and guide the synthetic efforts, in silico docking studies on compounds T_1AM and **1**−**10** were also performed in order to simulate the interaction of the synthesized compounds with the putative receptor-binding site. Given the absence of crystallographic data for the TAAR1 receptor, a theoretical model of the *m*TAAR1 receptor was built to carry out the docking studies.

Following a multidisciplinary approach, we identified two compounds, namely **2** and **3**, that are equipotent to endogenous thyronamines, and could represent suitable tools for studying the physiological roles of TAAR1 receptor using in vitro and/or in vivo models.

RESULTS AND DISCUSSION

Rational Design of New Compounds. The recent discovery that endogenous thyronamines (i.e., T0AM and T1AM) potently activate rat TAAR1 (*r*TAAR1) and mouse TAAR1 (*m*TAAR1) heterologously expressed in HEK293 cells, with T1AM being the most effective, spurred the discovery of the first rationally designed "superagonist" and antagonist compounds that target TAAR1.[25] In general, structural−activity relationship studies have led to the following conclusions: a basic amino group at Cα is required for activity, and monomethylation of the amine can be beneficial; an iodide or methyl substituent at the 3-position of the thyronamine scaffold is optimal for activity; the 4′-OH of thyronamine is not necessary for activity but its removal may render the remaining compound difficult to metabolize and possibly result in impaired clearance.

With the aim of enriching the number of selective ligands for TAAR1 and providing new tools to facilitate the understanding of TAAR1 physiological functions and therapeutic potential, in the present work we designed and synthesized a novel class of thyronamine analogues that are more synthetically accessible

DOI: 10.1021/acs.jmedchem.5b00526
J. Med. Chem. 2015, 58, 5096−5107

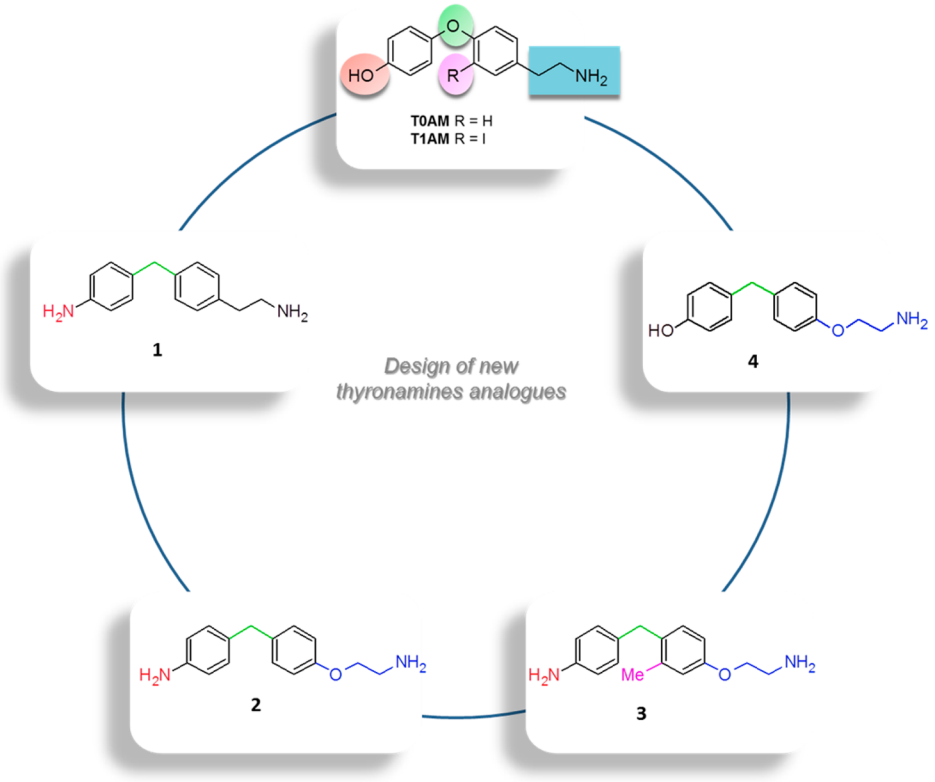

Figure 2. Medicinal chemistry strategies pursued in the design of new thyronamine analogues.

Scheme 1[a]

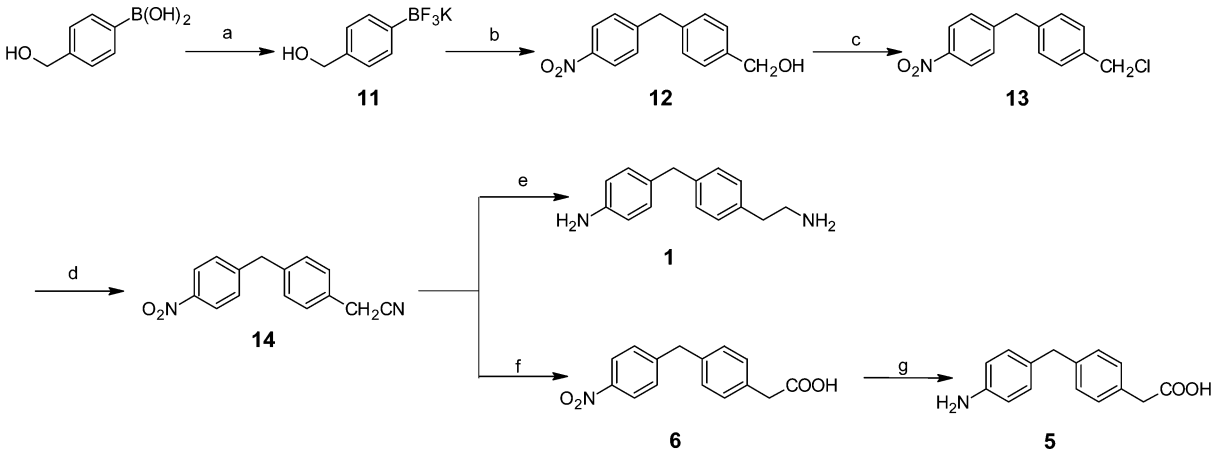

[a]Reagents and conditions: (a) KHF_2, $MeOH/H_2O$, rt, 30 °C; (b) 4-nitrobenzyl bromide, $PdCl_2$ dppf, Cs_2CO_3, H_2O/dioxane, 95 °C, 24 h; (c) $SOCl_2$, $CHCl_3$, rt, 2 h; (d) NaCN, H_2O/CH_3CN, mw; (e) $LiAlH_4$, $AlCl_3$, THF, reflux, 12 h; (f) H_2SO_4 50%, reflux, 30 °C; (g) hydrazine hydrate, carbon, $FeCl_3$, MeOH, reflux, 12 h.

than traditional thyronamines and have potentially useful receptor activation and functional properties.

It is well-known that biaryl-ether-forming reactions represent a significant problem in organic synthesis, and the biaryl-ether linkage in thyronamines requires the construction of both the appropriate boronic acid and phenol fragments throughout a multistep process.[26] Thus, taking advantage of our knowledge in the synthesis of analogues of thyroid hormones,[27] we first simplified the chemical synthesis of thyronamine analogues by replacing the oxygen bridging the aromatic rings with a methylene linkage. Subsequently, we examined the possibility of replacing the 4′-OH substituent of thyronamines with a bioisostere group, such as the 4′-NH_2, which retains the same H-bonding donor and acceptor capabilities of the OH group while also improving the pharmacokinetic properties of the molecule (i.e., solubility, hydrophilicity). Following this approach, we obtained the first oxygen free biaryl-methane thyronamine analogue **1** (Figure 2).

In addition, given the pharmacological survey by Bunzow et al.[8] showing that TAAR1 could be activated by aminergic G protein coupled receptor (GPCR) drugs with structurally diverse ethylamine segments, and knowing that the ethylamine side chain of thyronamines is exposed to rapid metabolic degradation by MAO,[23] we decided to synthesize new

DOI: 10.1021/acs.jmedchem.5b00526
J. Med. Chem. 2015, 58, 5096−5107

Scheme 2[a]

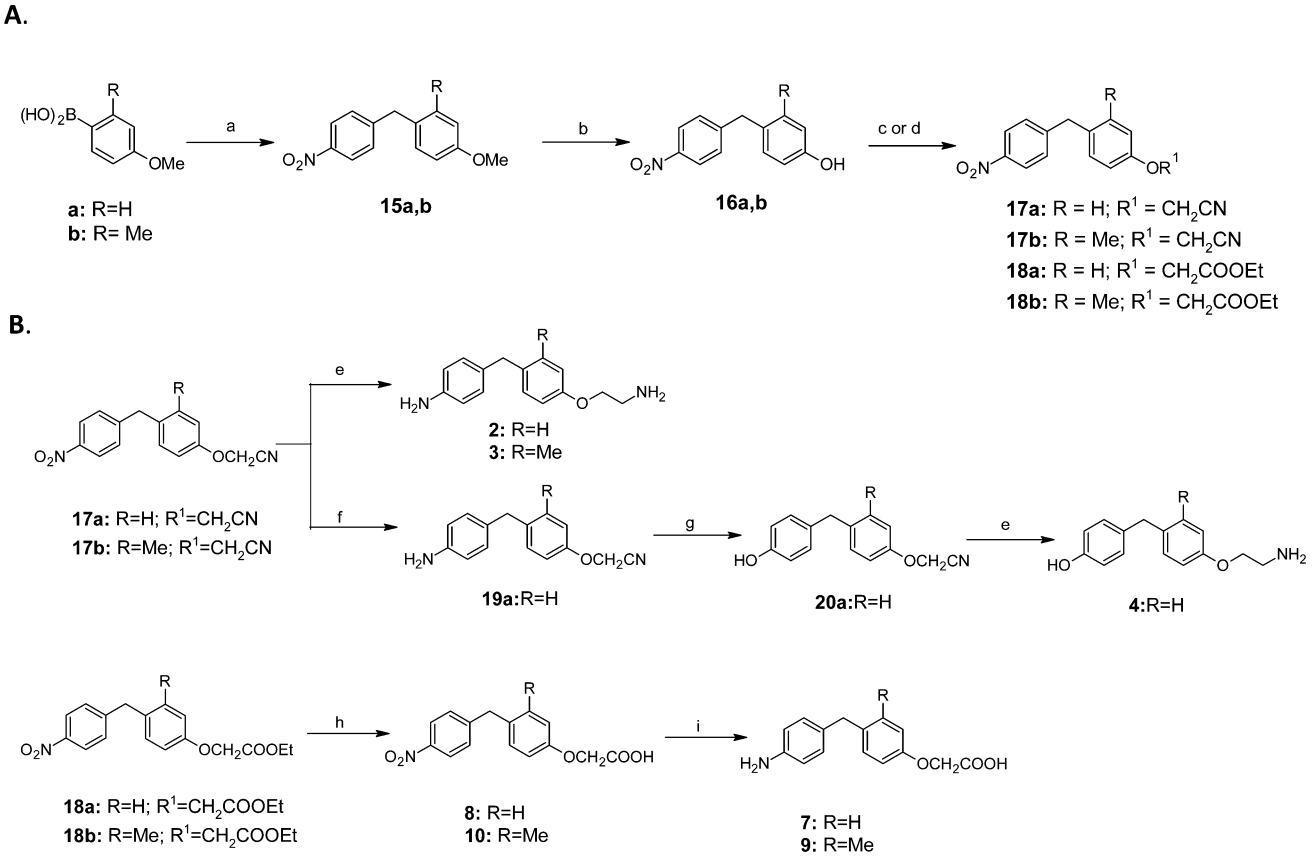

[a]Reagents and conditions: (a) 4-nitrobenzyl bromide, K_2CO_3, $PdCl_2$, acetone/H_2O, rt, 72 h; (b) BBr_3, DCM, 0 °C, 1 h; (c) $BrCH_2CN$, DMF, Cs_2CO_3, rt, 30 °C; (d) $BrCH_2COOEt$, DMF, Cs_2CO_3, rt, 30 °C; (e) $LiAlH_4$, $AlCl_3$, THF, reflux, 12 h; (f) H_2, Pd/C, AcOH, EtOH, rt, 12 h; (g) $NaNO_2$, H_2SO_4, H_2O, 100 °C, 1 h; (h) NaOH 10%, MeOH, reflux, 1 h; (i) hydrazine hydrate, Carbon, $FeCl_3$, MeOH, reflux, 12 h.

thyronamine analogues by replacing the ethylamine side chain with an aminoethoxy group. Thus, three new aminoethoxy analogues of our scaffold compound **1** were designed (Figure 2), with **2** and **4** being a close mimic of thyronamine (T0AM), whereas compound **3**, which has a methyl group at position 3, could be considered a new halogen-free 3-iodothyronamine (T1AM) analogue.

Oxidative deamination followed by aldehyde oxidation by ubiquitous enzyme aldehyde dehydrogenase is a major and rapid pathway of T1AM and T0AM metabolism, resulting in the production of the corresponding thyroacetic acids, namely TA_1 and TA_0[23] (Figure 1). This conversion could be significantly inhibited by treatment with the monamine oxidase (MAO) and semicarbazide-sensitive amine oxidase (SSAO) inhibitor, iproniazid.[23] Recent findings suggested that generation of TA_1 by deamination might contribute, at least in part, to the acute effects of T1AM in vivo and showed that oxidative deamination had a marked effect on T1AM pharmacokinetics.[20] Thus, to expand our SAR analysis on 4′-NH_2-biaryl-methane thyronamine analogues, we synthesized the corresponding deamination product of compounds **1**−**3**, namely **5**, **7**, and **9**, as well as their 4′-NO_2 analogues, namely **6**, **8**, and **10** (Figure 1).

Synthesis. Utilizing a divergent synthetic route, we synthesized the entire panel of new thyronamine analogues (**1**−**10**) from commercially available starting materials.

Palladium-catalyzed Suzuki−Miyaura coupling of *p*-nitrobenzyl bromide with selected phenyl boronic acid derivatives, either commercially available or easily generated in situ, was a crucial component to our synthetic route, and allowed efficient production of the key biaryl methane intermediates **12** and **15a,b** in only one to two steps. As shown in Scheme 1, starting from intermediate **12**, easily obtained by palladium(0)-catalyzed Suzuki−Miyaura cross-coupling reaction of the trifluoroborate salt **11** with 4-nitrobenzyl bromide,[28] the reaction with $SOCl_2$ followed by the nucleophilic substitution with NaCN gave the nitrile derivative **14**. The reduction of **14** with $LiAlH_4$ in the presence of a Lewis's acid afforded the diamine **1**, while its hydrolysis with H_2SO_4 50% provided the carboxylic acid **6**. The reduction of **6** with hydrazine hydrate in the presence of $FeCl_3$ and carbon provided the corresponding 4-(4-aminobenzyl)phenylacetic acid **5**.

Palladium(0)-catalyzed Suzuki−Miyaura cross-coupling reaction between the *p*-nitrobenzyl bromide and the appropriate 4-methoxyboronic acid provided the compound **15a,b** (Scheme 2A). The resulting adduct was treated with boron tribromide to obtain the phenolic derivative **16a,b**, which was then alkylated using bromoacetonitrile or ethyl bromoacetate, affording compound **17a,b** or **18a,b**, respectively. The final products **2** and **3** were obtained by reduction with $LiAlH_4/AlCl_3$ of **17a** and **17b**, respectively (Scheme 2B). The catalytic hydrogenation of **17a** followed by the reaction with $NaNO_2$ in H_2SO_4 gave the phenol **20a**, which was reduced with $LiAlH_4/AlCl_3$ to provide the desired product **4**. Finally, the cleavage of ethyl ester **18a,b** afforded the final products **8** and **10**, which were submitted to reduction with hydrazine hydrate in the presence of $FeCl_3$ and carbon to afford the amines **7** and **9**.

DOI: 10.1021/acs.jmedchem.5b00526
J. Med. Chem. 2015, 58, 5096−5107

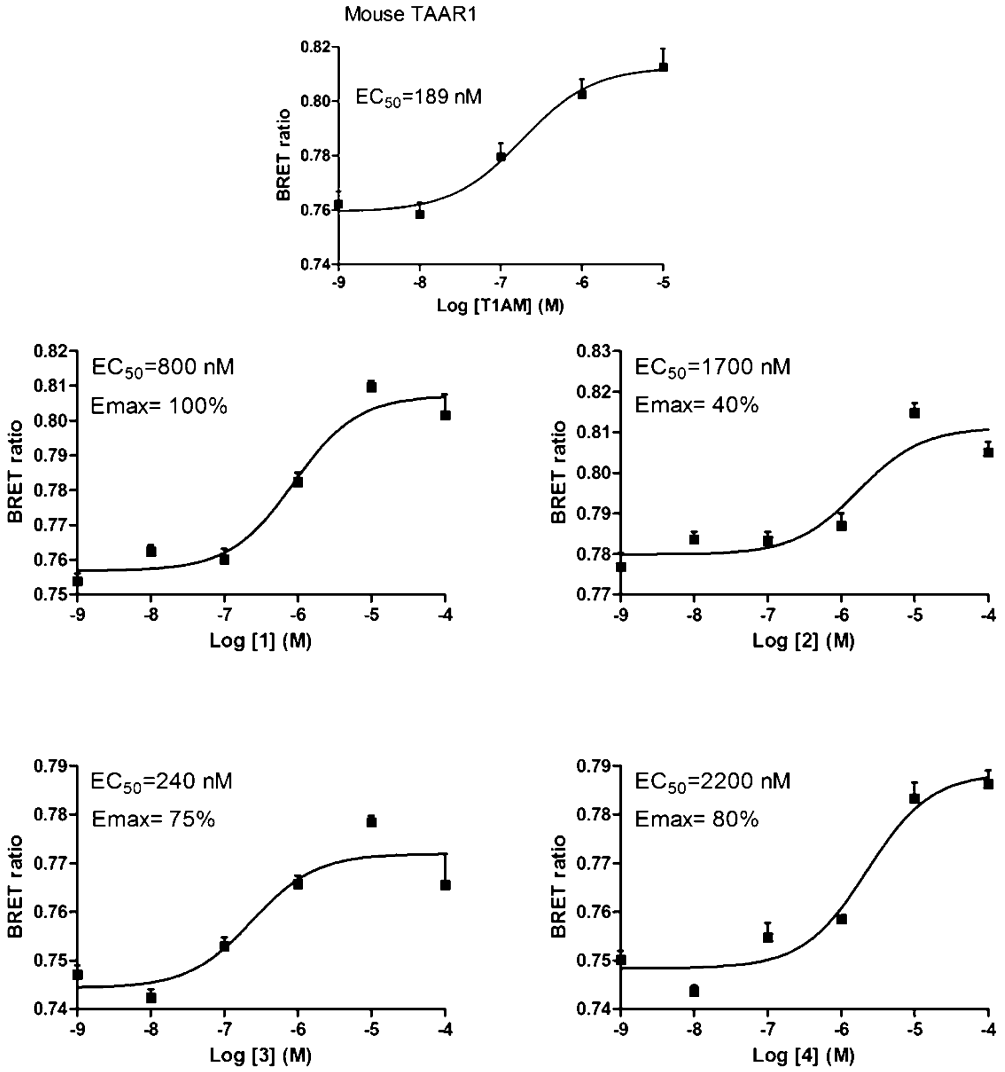

Figure 3. cAMP variations induced by the tested compounds in cells coexpressing *m*TAAR1 and EPAC. Cells were treated with the compounds at different concentrations and plotted as a dose−response experiment. Curve was fitted using a nonlinear regression and one site specific binding with GraphPad Prism5. Data are plotted as SEM of 4−5 independent experiments.

The newly designed compounds were then tested on the basis of the pharmacological responses originally described for T0AM and T1AM, namely cAMP production in HEK-293 cells expressing *m*TAAR1, induction of negative inotropic effect (reduced cardiac output) in isolated working rat heart preparations, and modulation of plasma glucose level in CD-1 mice.

Receptor Activation. As previously reported, both *r*TAAR1 and *m*TAAR1 are coupled to stimulatory G proteins and thus induce cAMP production in HEK293 stable cell lines upon agonist exposure.[8] We measured the activity of the new compounds using BRET-based assay[29] in which HEK293 cells were transfected with *m*TAAR1, or empty vector as control, and the cAMP BRET biosensor.[30] As reference compound, we used the standard TAAR1 agonist β-PEA that in our tests also increased cAMP through TAAR1 activation (EC_{50} = 138 nM). In the initial screening phase, all the compounds were tested at 10 μM either for agonistic or antagonistic activity. For the compounds that were found to be active, a dose response was then performed to calculate their corresponding EC_{50} values. After the initial phase, only the four biaryl-methane thyronamine analogues **1**−**4** were found to potently activate TAAR1. As shown in Figure 3, compounds **1**−**4** are effective TAAR1 agonists in HEK-293 cells transfected with *m*TAAR1, and compound **3**, which shares a close similarity to T1AM, was found to be the most potent (**3**: EC_{50} = 240 nM; T1AM EC_{50} = 189 nM). It is noteworthy that, even though **1** resulted to be less potent than **3** (EC_{50} = 800 nM), it shows the highest efficacy (E_{max} = 100%).

Heart Perfusion Experiments. It is already known that endogenous thyronamines (i.e., T0AM and T1AM) produced a reversible, dose-dependent negative inotropic effect in the isolated working rat heart preparations, and recent studies have shown the expression of mRNA coding for at least five different TAAR subtypes in rat heart, namely TAAR1−4 and TAAR8a, with the latter being quantitatively preponderant.[13,14] The T1AM corresponding synthetic analogue **3**, which has emerged from the TAAR1 activation study as the most potent derivative, and the T0AM relative synthetic compound **2**, were also examined in heart perfusion experiments. Freshly isolated adult rat hearts were perfused with buffer containing escalating doses of **2** or **3**, while the hemodynamic variables were monitored. **3** doses between 20 and 40 μM led to an immediate reduction in cardiac output (Figure 4).

DOI: 10.1021/acs.jmedchem.5b00526
J. Med. Chem. 2015, 58, 5096−5107

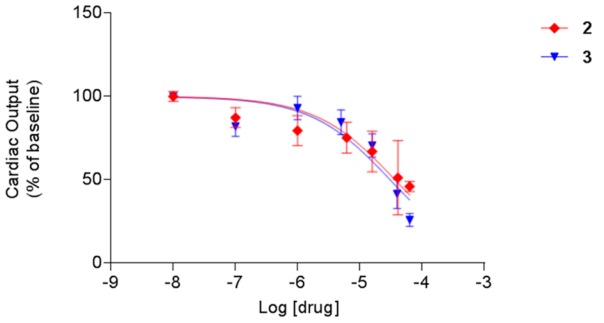

Figure 4. Dose–response curves for the effects of **2** (red) and **3** (blue) on cardiac output. Data points are values measured after 30 min of perfusion, expressed as percentage of baseline values. Bars are mean ± SE of 3–7 hearts per group. Results were analyzed by nonlinear regression using a sigmoidal dose response model to calculate the reported IC_{50}'s values.

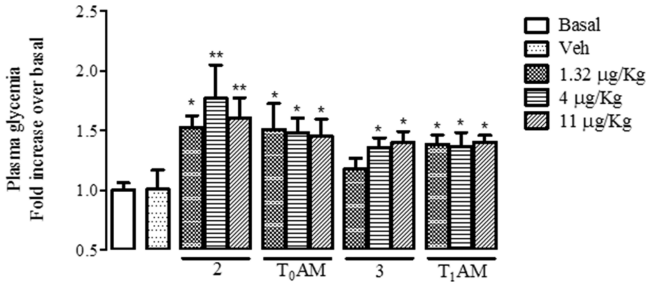

Figure 5. Effect of **2** and **3** on plasma glycaemia in comparison to T0AM and T1AM, respectively. *P < 0.05 vs vehicle. **P < 0.001 vs vehicle.

Within 10 min of receiving the highest **3** dose (40 μM), cardiac output dropped by 60%, as compared with controls, and remained at this rate for the duration of the experiment (1 h). The IC_{50} averaged 30 μM for the effect on cardiac output being almost comparable to previously observed T1AM IC_{50} value (i.e IC_{50} = 27 μM), while only minor effects were observed on heart rate. In isolated rat hearts with reduced inotropic drive resulting from pretreatment with **3**, administration of isoproterenol increased cardiac output (data not shown). This normalizing response to isoproterenol shows that β-adrenergic signaling is conserved in the presence of **3**, thus suggesting that the regulation of cardiac function is under the control of signaling pathways modulated by norepinephrine-sensitive and thyronamine-sensitive G protein coupled receptors (GPCRs). **2** treatment also resulted in a rapid reduction in cardiac output with no observable effect on heart rate, suggesting that also **2** is a negative inotropic agent with an IC_{50} of 34 μM, as compared with 30 μM for **3** (Figure 4).

Rat hearts were also perfused with buffer containing escalating doses (1–100 μM) of **7** and **9**, which represent the potential deamination product of **2** and **3**, respectively, but no effects on cardiac function were observed (data not shown).

Modulation of Plasma Glucose Level. T1AM has been reported to induce glucagon secretion and determine insulin secretion. These effects were observed with icv administration of T1AM dosages at low as 1.3 μg/kg,[19,20] but evidence for a peripheral action has also been reported at higher dosages.[21,31]

Consequently, the effects induced by **2** and **3** derivatives on plasma glucose level were also assessed. Figure 5 shows that a single low dose of **2** (1.32 μg/kg, ip) or **3** (4.0 μg/kg, ip) increases plasma glycaemia with a potency comparable to that of T0AM and T1AM, respectively.

Molecular Modeling. To explore the *m*TAAR1 binding site features, a homology model was built using the ligand-based homology modeling strategy proposed by Moro.[32] Briefly, the ligand-based homology modeling is performed by the proper handling of insertions and deletions of any selected extra-atoms during the energy tests and minimization stages of the modeling procedure. This computational option is very useful when one wishes to build a homology model in the presence of a ligand docked into the primary template and has been widely and fruitfully used by us to build GPCR as well as various enzyme models.[33,34] More specifically, in this work, the GPCR 3D structure was generated using 3PDS β_2-adrenoreceptor as template, following the procedure we previously applied for the development of the human TAAR1 model[33]

Similarly, the *m*TAAR1 model was built and refined in the presence of T1AM properly placed into the 3PDS β_2-adrenoreceptor binding site by docking procedures. In this way, we can safely assume that we were able to build a much better *m*TAAR1 binding site for the in silico analysis of the new derivatives than using standard homology modeling protocols. More specifically, starting from the derived β_2-adrenoreceptor/agonist complex, the *m*TAAR1 model was derived by aligning the *m*TAAR1 (Q923Y8) fast a sequence onto the 3PDS X-ray coordinates using the Blosum62 matrix implemented in MOE software (Figure 6a).

The reliability of the alignment was verified by the high value of the pairwise percentage residue identity (PPRI = 33%). Accordingly, a consistent number of *m*TAAR1 residues resulted to be conserved in comparison with those of the β_2-adrenoreceptor TM helices: (i) M29, L31, L34, G39, V43, I47, S30, I32, A35, N40, I44, F50, and L53 in TM1; (ii) T57, N58, S63, A65, D68, G72, and P77 in TM2; (iii) C95, T99, S100, D102, A108, S109, I110, L113, I116, D119, R120, and Y121 in TM3 (the DRY motif; 119–121 residues); (iv) V141, I143, L144, W147, F155, and I157 in TM4; (v) A193, S197, F198, Y199, P201, M205, F207, V208, Y209, R211, A216, and K217 in TM5; (vi) K242, E243, K245, A246, K248, T249, L250, G251, I252, G255, F257, C260, W261, P263, F264, and F265 in TM6 (CWXP motif; 260–263 residues); (vii) L286, W288, G290, Y291, N293, S294, N297, P298, and Y301 in TM7.

The derived backbone conformation was inspected by Ramachandran plot (showing absence of outliers) and superimposed to the coordinates of the template structure (RMSD = 0.459 Å; Figure 6b).

Subsequently, we used our *m*TAAR1 model to perform docking studies on the reference compound T_1AM and on **1**–**10** derivatives.

On the basis of our calculations, T_1AM proved to be highly stabilized into the receptor binding site by two H-bonds between the protonated amine group and the D102 and Y291 side chains and also by one H-bond between the phenolic hydroxyl group and the R82 backbone carbonyl moiety. Furthermore, the T1AM protonated amine group is able to establish additional cation–π contacts with Y287 and with the aforementioned Y291. Notably, the central ether oxygen seems not to be involved in any significant amino acid interaction (Figure 6c).

The **2**, **3** and **1**, **4** derivatives partially shared the T1AM docking mode, described above. In particular, **3** (being the most active of this series) displayed: (i) two H-bonds between the

DOI: 10.1021/acs.jmedchem.5b00526
J. Med. Chem. 2015, 58, 5096–5107

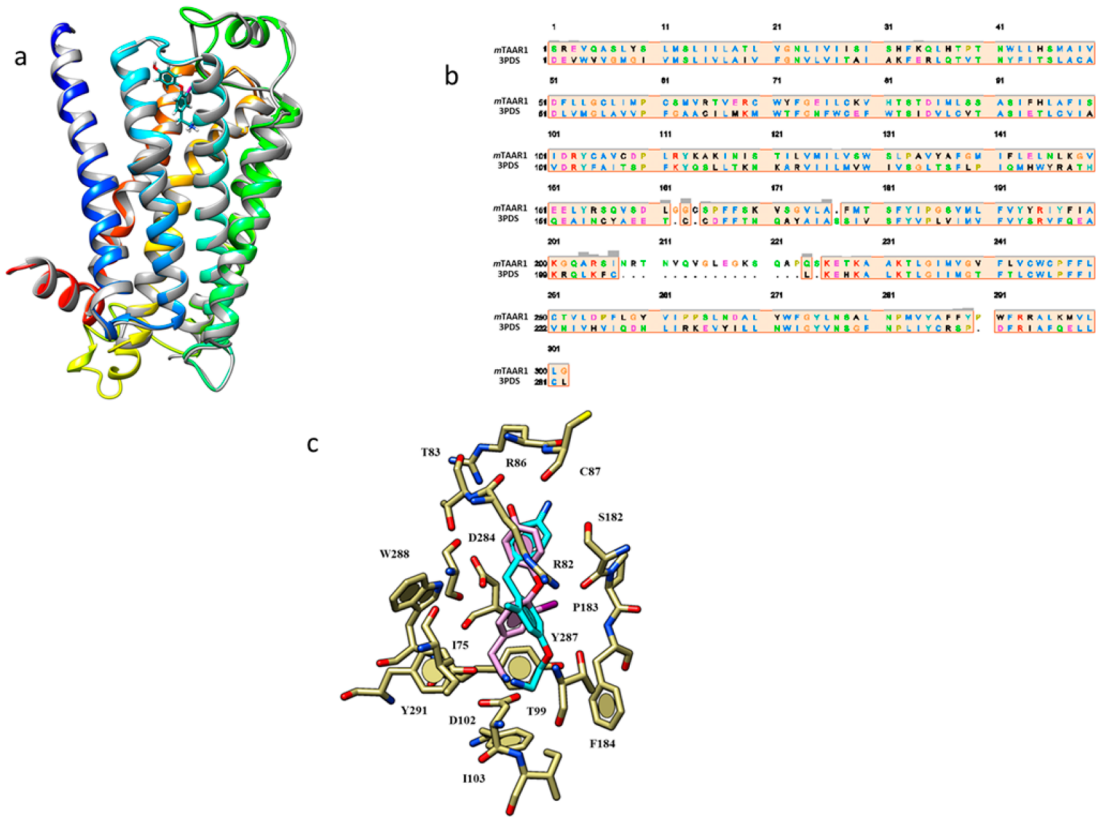

Figure 6. (a) The superimposition of the final *m*TAAR1 model (backbone colored by rainbow) on the 3PDS coordinates (backbone in gray) is depicted. The T1AM structure is also reported in stick (colored by atom type; *C* atom, cyan). (b) Sequence alignment of the *m*TAAR1 on the basis of the human β_2-adrenoreceptor (PDB 3PDS) coordinated. (c) Docking mode of the T_1AM and of thyronamine analogue **3** into the putative *m*TAAR1 binding site. The ligands are reported in stick, colored by atom type (C atom, pink and cyan, respectively).

protonated amine group and the D102 and Y291 side chains, (ii) cation−π interactions between the same group and Y291, and (iii) π−π stacking between the 4-(2-aminoethyloxy)phenyl group of the molecule and Y287 (Figure 6c). In addition, the aniline portion projects toward the R86 side chain, establishing cation−π interactions, while no H-bonds with the R82 backbone oxygen atom were detected. Notably, it could be hypothesized that the presence of an oxygen atom (amino-ethoxy portion) switched the ligand conformer toward the T99 side chain, causing a slightly different docking mode in comparison with that observed for T1AM.

CONCLUSIONS

Our efforts to identify potent and selective TAAR1 agonists synthetically more accessible than traditional thyronamines led to the identification of a family of diphenylmethane derivatives. By changing the biaryl-ether linkage present in thyronamines to a methylene linkage, we were able to use an efficient C−C bond forming reaction in the key biaryl-coupling step. This process is amenable of extensive customization, suggesting that a great variety of thyronamine structural variants will be accessible through this synthetic strategy. Analysis of the in vitro TAAR1 activity data reported herein showed that the following structural modifications are well tolerated by *m*TAAR1: (i) replacement of the phenol hydroxyl with an amino group, (ii) increase of the distance between the charged amine and the aromatic ring by inserting an oxygen bridge, and (iii) replacement of the 3-iodo substituent with an alkyl group (i.e., CH_3). Compounds **2** and **3** were found to be approximately equipotent to T0AM and T1AM, respectively. When administered to mice at a single dose of 1.32 and 3.4 μg/kg, both compounds increased plasma glycaemia with a potency comparable to that of the corresponding parent compound. In addition, **2** and **3** revealed to be both potent negative inotropic agents, with **3** being only slightly more potent than **2**.

EXPERIMENTAL SECTION

Chemistry. *General Material and Methods.* Melting points were determined on a Kofler hot-stage apparatus and are uncorrected. Chemical shifts (δ) are reported in parts per million downfield from tetramethylsilane and referenced from solvent references; coupling constants *J* are reported in hertz. ^{1}H NMR and ^{13}C NMR spectra of all compounds were obtained with a Varian Gemini 200 MHz or with a Bruker TopSpin 3.2 400 MHz spectrometer. ^{13}C NMR spectra were fully decoupled. The following abbreviations are used: singlet (s), doublet (d), triplet (t), double−doublet (dd), and multiplet (m). The elemental compositions of the compounds agreed to within ±0.4% of the calculated values. Chromatographic separation was performed on silica gel columns by flash (Kieselgel 40, 0.040−0.063 mm; Merck) or gravity column (Kieselgel 60, 0.063−0.200 mm; Merck) chromatography. The ≥95% purity of the tested compounds was confirmed by combustion analysis. Reactions were followed by thin-layer chromatography (TLC) on Merck aluminum silica gel (60 F_{254}) sheets that were visualized under a UV lamp. The microwave-assisted procedures were carried out with a CEM Discover LabMate microwave. Evaporation was performed in vacuo (rotating evaporator). Sodium sulfate was always used as the drying agent. Commercially available chemicals were purchased from Sigma-Aldrich.

4-(4-(2-Aminoethyl)benzyl)aniline (1). To a suspension of $LiAlH_4$ (115.4 mg, 3.04 mmol) in THF was added dropwise a solution of $AlCl_3$ (405 mg, 3.04 mmol) in THF (200 mL), and the mixture was

DOI: 10.1021/acs.jmedchem.5b00526
J. Med. Chem. 2015, 58, 5096−5107

stirred for 5 min at rt. A solution of **14** (85.0 mg, 0.34 mmol) in THF was added dropwise, and the mixture was heated at reflux for 12 h. The mixture was cooled to 0 °C with an ice bath and added dropwise with water and then with 10% aqueous HCl. The mixture was extracted with diethyl ether, and the aqueous layer was made alkaline with 2N aqueous NaOH and extracted with $CHCl_3$. The organic phase was separated, washed with brine, dried, filtered, and concentrated. The crude product was purified by conversion to the corresponding hydrochloride salt. White solid; mp 165−167 °C (70% yield). ^{1}H NMR (CD_3OD): δ 2.93 (t, 2H, J = 7.8 Hz, CH_2), 3.15 (t, 2H, J = 7.8 Hz, CH_2), 4.02 (s, 2H, CH_2), 7.25−7.20 (m, 4H, Ar), 7.33 (d, 2H, J = 8.4 Hz, Ar), 7.38 (d, 2H, J = 8.4 Hz, Ar) ppm. ^{13}C NMR (CD_3OD): δ 142.83, 139.53, 134.58, 130.20, 129.12, 128.67, 128.50, 122.71, 40.54, 40.30, 32.75 ppm. Anal. ($C_{15}H_{18}N_2$) C, H, N % Calcd: 79.61 (C), 8.02 (H), 12.38 (N). % Found: 79.45 (C), 8.18 (H), 12.77 (N).

*4-(4-(2-Aminoethoxy)benzyl)aniline (**2**).* Compound **2** was synthesized from **17a** (96.3 mg, 0.34 mmol), $LiAlH_4$ (3.04 mmol), and $AlCl_3$ (405 mg, 3.04 mmol) in THF (200 mL) following the same procedure described above for the preparation of **1**. The crude was purified by conversion in the corresponding hydrochloride salt. White solid; mp 137−135 °C (70% yield). ^{1}H NMR (CD_3OD): δ 3.35 (t, 2H, J = 5.0 Hz, CH_2), 3.93 (s, 2H, CH_2), 4.20 (t, 2H, J = 5.0 Hz, CH_2NH_2), 6.94 (d, 2H, J = 8.6 Hz, Ar), 7.16 (d, 2H, J = 8.3, Hz, Ar), 7.15 (d, 2H, J = 8.6 Hz, Ar), 7.26 (d, 2H, J = 8.3 Hz, Ar), ppm. ^{13}C NMR (CD_3OD): δ 158.13, 141.85, 135.52, 133.72, 131.24, 131.02, 122.40, 115.81, 65.32, 41.21, 40.39 ppm. Anal. ($C_{16}H_{21}ClN_2O$) C, H, N % Calcd: 65.63 (C), 7.23 (H), 9.57 (N). % Found: 65.61 (C), 7.52 (H), 9.73 (N).

*4-(4-(2-Aminoethoxy)-2-methylbenzyl)aniline (**3**).* Compound **3** was synthesized from **17b** (101 mg, 0.34 mmol), $LiAlH_4$ (3.04 mmol), and $AlCl_3$ (405 mg, 3.04 mmol) in THF (200 mL) following the same procedure described above for the preparation of 1. The crude was purified by conversion in the corresponding hydrochloride salt. White solid; mp 156−158 °C (75% yield). ^{1}H NMR (CD_3OD): δ 2.18 (s, 3H, CH_3), 3.36 (t, 2H, J = 4.0 Hz, CH_2), 4.00 (s, 2H, CH_2), 4.21 (t, 2H, J = 4.0 Hz, CH_2NH_2), 6.79−6.88 (m, 2H, Ar), 7.11 (d, 1H, J = 8.0 Hz, Ar), 7.28−7.34 (m, 4H, Ar) ppm. ^{13}C NMR (CD_3OD): δ 158.32, 143.87, 139.32, 132.78, 132.22, 131.27, 129.71, 124.01, 117.86, 113.05, 65.23, 40.41, 38.89, 19.93 ppm. Anal. ($C_{15}H_{19}ClN_2O$) C, H, N % Calcd: 64.63 (C), 6.87 (H), 10.05 (N). % Found: 64.74 (C), 7.02 (H), 9.95 (N).

*4-(4-(2-Aminoethoxy)benzyl)phenol (**4**).* Compound **4** was synthesized from **20a** (32.3 mg, 0.13 mmol), $LiAlH_4$ (1.21 mmol), and $AlCl_3$ (161 mg, 1.21 mmol) in THF (200 mL) following the same procedure described above for the preparation of **1**. The crude product was purified by conversion to the corresponding hydrochloride salt. White solid; mp 175−177 °C (50% yield). ^{1}H NMR (CD_3OD): δ 3.34 (t, 2H, J = 4.8 Hz, CH_2), 3.80 (s, 2H, CH_2), 4.20 (t, 2H, J = 4.8 Hz, CH_2NH_2), 6.68 (d, 2H, J = 8.4 Hz, Ar), 6.91 (d, 2H, J = 8.8 Hz, Ar), 6.97 (d, 2H, J = 8.4 Hz, Ar), 7.11 (d, 2H, J = 8.8 Hz Ar) ppm. ^{13}C NMR (CD_3OD): δ 156.62, 136.83, 133.80, 130.88, 130.71, 116.15, 115.61, 65.30, 41.07, 40.40 ppm. Anal. ($C_{15}H_{17}NO_2$) C, H, N % Calcd: 74.05 (C), 7.04 (H), 5.76 (N). % Found: 74.31 (C), 7.22 (H), 5.73 (N).

*2-(4-(4-Aminobenzyl)phenyl)acetic Acid (**5**).* To a solution of **6** (167 mg, 0.64 mmol) in MeOH (50 mL) was added carbon (33.7 mg) and $FeCl_3$ (7 mg). The reaction mixture was warmed to 60 °C, then hydrazine monohydrate was added dropwise (0.33 mL, 6.71 mmol). The mixture was refluxed overnight then filtered on a Celite pad and the solvent removed. The residue was dissolved in AcOEt and washed with water. The organic layer was dried and evaporated under reduced pressure. The crude was purified by conversion in the corresponding hydrochloride salt. White solid; mp 154−156 °C (72% yield). ^{1}H NMR (CD_3OD): δ 3.61 (s, 2H, CH_2), 4.01 (s, 2H, CH_2), 7.19 (d, 2H, J = 8.0 Hz, Ar), 7.26 (d, 2H, J = 8.0 Hz, Ar), 7.31 (d, 2H, J = 8.4 Hz, Ar), 7.37 (d, 2H, J = 8.4 Hz, Ar) ppm. ^{13}C NMR (CD_3OD): δ 175.61, 144.37, 144.32, 140.46, 134.15, 131.60, 130.65, 130.60, 130.03, 129.98, 129.80, 129.37, 124.04, 41.69, 41.42 ppm. Anal. ($C_{15}H_{13}NO_4$·HCl) C, H, N % Calcd: 64.87 (C), 5.81 (H), 5.04 (N). % Found: 64.72 (C), 5.92 (H), 5.09 (N).

*2-(4-(4-Nitrobenzyl)phenyl)acetic Acid (**6**).* A solution of **14** (51.6 mg, 0.20 mmol) in 50% H_2SO_4 (0.2 mL) was placed under stirring at reflux for 30 min. After cooling, the water was added and the solid precipitate was collected to give **6**. Yellow solid; mp 175−177 °C (79% yield). ^{1}H NMR ($CDCl_3$): δ 3.58 (s, 2H, CH_2), 4.09 (s, 2H, CH_2), 7.19 (d, 2H, J = 7.6 Hz, Ar), 7.37−7.27 (m, 4H, Ar), 8.17 (d, 2H, J = 7.6 Hz, Ar) ppm. ^{13}C NMR ($CDCl_3$): δ 173.69, 148.41, 146.52, 138.46, 133.08, 129.77, 129.59, 129.51, 129.08, 123.75, 123.69, 42.65, 41.25 ppm. Anal. ($C_{15}H_{13}NO_4$) C, H, N % Calcd: 66.41 (C), 4.83 (H), 5.16 (N). % Found: 66.44 (C), 4.55 (H), 5.28 (N).

*2-(4-(4-Aminobenzyl)phenoxy)acetic Acid (**7**).* Compound **7** was synthesized from **8** (184.0 mg, 0.64 mmol), hydrazine monohydrate (6.71 mmol), carbon (33.7 mg), and $FeCl_3$ (7 mg) in MeOH (50 mL) following the same procedure described above for the preparation of **5**. The residue was dissolved in AcOEt and washed with water. The organic layer was dried and evaporated under reduced pressure. White solid; mp 153−155 °C (70% yield). ^{1}H NMR ($CDCl_3$): δ 3.82 (s, 2H, CH_2), 4.54 (s, 2H, CH_2), 6.62 (d, 2H, J = 8.4 Hz, Ar), 6.81 (d, 2H, J = 8.4 Hz, Ar), 6.95 (d, 2H, J = 8.4 Hz, Ar), 7.11 (d, 2H, J = 8.4 Hz Ar) ppm. ^{13}C NMR ($CDCl_3$): δ 168.76, 155.34, 144.52, 135.92, 131.22, 130.04, 129.65, 115.34, 114.49, 67.09, 40.14 ppm. Anal. ($C_{15}H_{15}NO_3$) C, H, N % Calcd: 70.02 (C), 5.88 (H), 5.44 (N). % Found: 70.39 (C), 5.93 (H), 5.59 (N).

*2-(4-(4-Nitrobenzyl)phenoxy)acetic Acid (**8**).* To a solution of the ester **18a** (179.7 mg, 0.57 mmol) in MeOH was added dropwise an aqueous solution of NaOH 10% (0.2 mL), the resulting solution was refluxed for 30 min, then, after cooling, the solvent was evaporated. The residue was acidified to pH 3 with HCl 1N, and the precipitate was filtered off, washed with H_2O, and dried. White solid; mp 162−164 °C (87% yield). ^{1}H NMR ($CDCl_3$): δ 4.02 (s, 2H, CH_2), 4.66 (s, 2H, CH_2), 6.88 (d, 2H, J = 8.4 Hz, Ar), 7.11 (d, 2H, J = 8.4 Hz, Ar), 7.31 (d, 2H, J = 8.4 Hz, Ar), 8.14 (d, 2H, J = 8.4 Hz Ar) ppm. ^{13}C NMR (200 MHz, $CDCl_3$) δ: 158.60, 146.30, 130.22, 129.56, 128.00, 123.79, 123.15, 115.03, 77.35, 64.89, 29.70 ppm. Anal. ($C_{15}H_{13}NO_5$) C, H, N % Calcd: 62.72 (C), 4.56 (H), 4.88 (N). % Found: 62.91 (C), 4.23 (H), 4.59 (N).

*2-(4-(4-Aminobenzyl)-3-methylphenoxy)acetic Acid (**9**).* Compound **9** was synthesized from **10** (192.8 mg, 0.64 mmol), hydrazine monohydrate (6.71 mmol), carbon (33.7 mg), and $FeCl_3$ (7 mg) in MeOH (50 mL) following the same procedure described above for the preparation of **5**. The residue was dissolved in AcOEt and washed with water. The organic layer was dried and evaporated under reduced pressure. The crude was purified by conversion in the corresponding hydrochloride salt. White solid; mp 175−177 °C (65% yield). ^{1}H NMR (CD_3OD): δ 2.16 (s, 3H, CH_3), 3.77 (s, 2H, CH_2), 4.36 (s, 2H, CH_2), 6.57−6.80 (m, 4H, Ar), 6.81−6.89 (m, 2H, Ar) 6.92−7.01 (m, 2H, Ar) ppm. Anal. ($C_{16}H_{17}NO_3$) C, H, N % Calcd 70.83 (C), 6.32 (H), 5.16 (N). % Found. 70.90 (C), 6.37 (H), 5.29 (N).

*2-(3-Methyl-4-(4-nitrobenzyl)phenoxy)acetic Acid (**10**).* Compound **10** was synthesized from **18b** (187.7 mg, 0.57 mmol) and an aqueous solution of NaOH 10% (0.2 mL) in MeOH following the same procedure described above for the preparation of **8**. The residue was acidified to pH 3 with HCl 1N, and the precipitate was filtered off, washed with H_2O, and dried. White solid; mp 166−168 °C (90% yield). ^{1}H NMR ($CDCl_3$): δ 2.17 (s, 3H, CH_3), 4.02 (s, 2H, CH_2), 4.68 (s, 2H, CH_2), 6.70−6.80 (m, 2H, Ar), 7.03 (d, 1H, J = 8.2 Hz, Ar), 7.24 (d, 2H, J = 7.9 Hz, Ar), 8.12 (d, 2H, J = 7.9 Hz, Ar) ppm. ^{13}C NMR ($CDCl_3$) δ: 156.46, 148.56, 138.54, 131.33, 131.10, 130.88, 129.42, 123.84, 117.27, 112.04, 77.80, 64.93, 38.73, 20.06 ppm. Anal. ($C_{16}H_{15}NO_5$) C, H, N % Calcd: 63.78 (C), 5.02 (H), 4.65 (N). % Found: 63.87 (C), 5.21 (H), 4.51 (N).

*Potassium Trifluoro(4-(hydroxymethyl)phenyl)borate (**11**).* To a round-bottomed flask containing the 4-(hydroxymethyl)-phenylboronic acid (1.3 g, 8.55 mmol) in MeOH was added a solution of KHF_2 (2.7 g, 34.2 mmol) in distilled water at 0 °C. The mixture was stirred for 2 h, at rt, and then the solvent was completely removed under reduced pressure. The crude product was purified by crystallization from iPrOH to give **11**. White solid (63% yield). ^{1}H NMR (CD_3OD): δ 4.53 (s, 2H, CH_2), 7.18 (d, 2H, J = 7.2 Hz, Ar),

DOI: 10.1021/acs.jmedchem.5b00526
J. Med. Chem. 2015, 58, 5096−5107

7.48 (d, 2H, J = 7.2 Hz, Ar) ppm. Anal. ($C_7H_7BF_3KO$) C, H, N % Calcd: 39.28 (C), 3.30 (H). % Found: 39.55 (C), 3.43 (H).

*(4-(4-Nitrobenzyl)phenyl)methanol (**12**).* To a solution of trifluoroborane salt **11** (509 mg, 2.38 mmol) in dioxane/H_2O 9:1 (4 mL) was added, under nitrogen atmosphere, *p*-nitrobenzyl bromide (513 mg, 2.38 mmol), cesium carbonate (2.30 g, 7.1 mmol), and $PdCl_2$(dppf) (34.8 mg, 0.05 mmol). The resulting mixture was stirred at 95 °C for 24 h in a sealed vial. The crude mixture was evaporated and then diluted with water and extracted with DCM. The organic phase was dried over sodium sulfate and the solvent removed. The crude product was chromatographed on a silica gel column, eluting with *n*-hexane/AcOEt (70:30). White oil (32% yield). ^{1}H NMR ($CDCl_3$): δ 4.08 (s, 2H, CH_2), 4.68 (s, 2H, CH_2OH), 7.17 (d, 2H, J = 8.0 Hz Ar), 7.34−7.32 (m, 4H, Ar), 8.14 (d, 2H, J = 8.4 Hz, Ar) ppm. Anal. ($C_{14}H_{13}NO_3$) C, H, N. % Calcd: 69.12 (C), 5.39 (H), 5.76 (N) % Found: 69.03 (C), 5.63 (H), 5.58 (N).

*1-(Chloromethyl)-4-(4-nitrobenzyl)benzene (**13**).* To a solution of **12** (86.4 mg, 0.35 mmoli) in $CHCl_3$ at 0 °C was added $SOCl_2$ (3.50 mmol, 0.25 mL). The reaction mixture was stirred for 2 h at room temperature, then the solvent was evaporated. The residue was dissolved in H_2O and alkalized with NaOH 1N, and the aqueous layer was extracted with DCM. The organic phase was dried and the solvent was evaporated to give **13**, which was used without further purification. Yellow oil (83% yield). ^{1}H NMR ($CDCl_3$): δ 4.08 (s, 2H, CH_2), 4.57 (s, 2H, CH_2), 7.17 (d, 2H, J = 8.0 Hz, Ar), 7.35−7.32 (m, 4H, Ar), 8.15 (d, 2H, J = 8.8 Hz Ar) ppm. Anal. ($C_{14}H_{12}ClNO_2$) C, H, N. % Calcd: 64.25 (C), 4.62 (H), 5.35 (N). % Found: 63.96 (C), 4.46 (H), 5.71 (N).

*2-(4-(4-Nitrobenzyl)phenyl)acetonitrile (**14**).* To a solution of **13** (152 mg, 0.58 mmol) in CH_3CN (0.78 mL) was added NaCN (57.0 mg, 1.16 mmol) in H_2O (0.26 mL). The mixture was submitted to microwave irradiation (150W, 100 °C, 20 min). After cooling, the solution was extracted with DCM. Organic phase was dried and evaporated to dryness. Yellow oil (86% yield). ^{1}H NMR ($CDCl_3$): δ 3.73 (s, 2H, CH_2), 4.08 (s, 2H, CH_2), 7.19 (d, 2H, J = 8.0 Hz, Ar), 7.33−7.28 (m, 4H, Ar), 8.15 (d, 2H, J = 8.8 Hz, Ar) ppm. Anal. ($C_{15}H_{12}N_2O_2$) C, H, N % Calcd: 71.42 (C), 4.79 (H), 11.10 (N). % Found: 71.56 (C), 4.64 (H), 11.33 (N).

*General Procedure for Synthesis of Compounds **15a,b**.* To a solution of arylboronic acid (2.63 mmoli) in acetone/H_2O 1:1 (4 mL) was added, under nitrogen flux, *p*-nitrobenzyl bromide (569 mg, 2.63 mmol), K_2CO_3 (1.24 g, 6.58 mmol), and a catalytic amount of $PdCl_2$. The resulting mixture was stirred at rt for 62 h in a sealed vial. The crude mixture was evaporated and then diluted with water and extracted with Et_2O. The organic phase was dried over sodium sulfate and concentrated under vacuum.

*1-Methoxy-4-(4-nitrobenzyl)benzene (**15a**).* The crude residue was purified by column chromatography *n*-hexane/AcOEt (97:3), affording **15a** (47% yield). Yellow oil. ^{1}H NMR ($CDCl_3$): δ 3.79 (s, 3H, OCH_3), 4.02 (s, 2H, CH_2), 6.86 (d, 2H, J = 8.3 Hz, Ar), 7.10 (d, 2H, J = 8.3 Hz, Ar), 7.32 (d, 2H, J = 8.3 Hz, Ar), 8.13 (d, 2H, J = 8.3 Hz, Ar) ppm. Anal. ($C_{14}H_{13}NO_3$) C, H, N % Calcd: 69.12 (C), 5.39 (H), 5.76 (N). % Found: 69.21 (C), 5.43 (H), 5.98 (N).

*4-Methoxy-2-methyl-1-(4-nitrobenzyl)benzene (**15b**).* The crude residue was purified by column chromatography *n*-hexane/AcOEt (97:3), affording **15b** (49% yield). Yellow oil. ^{1}H NMR ($CDCl_3$): δ 2.15 (s, 3H, CH_3), 3.78 (s, 3H, OCH_3), 4.01 (s, 2H, CH_2), 6.69−6.80 (m, 2H, Ar), 7.01 (s, 1H, Ar), 7.23 (d, 2H, J = 8.4 Hz, Ar), 8.10 (d, 2H, J = 8.4 Hz, Ar) ppm. Anal. ($C_{15}H_{15}NO_3$) C, H, N % Calcd: 70.02 (C), 5.88 (H), 5.44 (N). % Found: 70.22 (C), 5.93 (H), 5.62 (N).

*General Procedure for Synthesis of Compounds **16a,b**.* A solution of **15a,b** (0.39 mmol) in anhydrous DCM (1.5 mL) was cooled to −78 °C and treated dropwise with a solution of BBr_3 in DCM (3.94 mL, 1.24 mmol), and the resulting solution was stirred at the same temperature for 5 min and at 0 °C for 1 h. The mixture was then diluted with water and extracted with DCM. Organic phase was dried and evaporated to give the products **16a** or **16b**.

*4-(4-Nitrobenzyl)phenol (**16a**).* White oil (95% yield). ^{1}H NMR ($CDCl_3$): δ 4.00 (s, 2H, CH_2), 6.78 (d, 2H, J = 7.5 Hz, Ar), 7.04 (d, 2H, J = 7.5 Hz, Ar) 7.32 (d, 2H, J = 7.9 Hz, Ar), 8.14 (d, 2H, J = 7.9 Hz, Ar) ppm. Anal. ($C_{13}H_{11}NO_3$) C, H, N % Calcd: 68.11 (C), 4.84 (H), 6.11 (N). % Found: 68.29 (C), 4.96 (H), 6.29 (N).

*3-Methyl-4-(4-nitrobenzyl)phenol (**16b**).* Pale-yellow oil (64% yield). ^{1}H NMR ($CDCl_3$): δ 2.13 (s, 3H, CH_3), 4.00 (s, 2H, CH_2), 6.65−6.59 (m, 2H, Ar), 6.96 (s, 1H, Ar), 7.24 (d, 2H, J = 7.9 Hz, Ar), 8.11 (d, 2H, J = 7.9 Hz, Ar) ppm. Anal. ($C_{14}H_{13}NO_3$) C, H, N % Calcd: 69.12 (C), 5.39 (H), 5.76 (N). % Found: 69.33 (C), 5.51 (H), 5.82 (N).

*General Procedure for Synthesis of Compounds **17a,b**.* To a mixture of cesium carbonate (725 mg, 2.22 mmol) and phenol **16a,b** (0.44 mmol) in 50 mL of DMF was added $BrCH_2CN$ (0.03 mL, 0.44 mmol). The reaction mixture was stirred for 30 min at rt, poured into 100 mL of cold HCl 1N, and extracted with AcOEt. The organic phase was dried and evaporated.

*2-(4-(4-Nitrobenzyl)phenoxy)acetonitrile (**17a**).* The crude product was purified by chromatography eluting with *n*-hexane/AcOEt (70:30). White oil (96% yield). ^{1}H NMR ($CDCl_3$): δ 4.05 (s, 2H, CH_2), 4.76 (s, 2H, CH_2), 6.94 (d, 2H, J = 8.6 Hz, Ar), 7.15 (d, 2H, J = 8.6 Hz, Ar), 7.31 (d, 2H, J = 8.6 Hz, Ar), 8.14 (d, 2H, J = 8.6 Hz, Ar) ppm. Anal. ($C_{15}H_{12}N_2O_3$) C, H, N. % Calcd: 67.16 (C), 4.51 (H), 10.44 (N). % Found: 67.24 (C), 4.72 (H), 10.62 (N).

*2-(3-Methyl-4-(4-nitrobenzyl)phenoxy)acetonitrile (**17b**).* The crude product was purified by chromatography eluting with *n*-hexane/AcOEt (70:30). White oil (98% yield). ^{1}H NMR ($CDCl_3$): δ 2.19 (s, 3H, CH_3), 4.03 (s, 2H, CH_2), 4.76 (s, 2H, CH_2), 6.81−6.77 (m, 2H, Ar), 7.08 (s, 1H, Ar), 7.25 (d, 2H, J = 8.6 Hz, Ar), 8.13 (d, 2H, J = 8.6 Hz, Ar) ppm. Anal. ($C_{16}H_{14}N_2O_3$) C, H, N % Calcd: 68.07 (C), 5.00 (H), 9.92 (N). % Found: 68.21 (C), 5.11 (H), 9.86 (N).

*General Procedure for Synthesis of Compounds **18a,b**.* Compound **18a,b** was synthesized from **16a,b** (0.44 mmol) and $BrCH_2COOEt$ (73.5 mg, 0.44 mmol) in DMF (1.2 mL) following the same procedure as described above for the preparation of **17a,b**

*Ethyl 2-(4-(4-Nitrobenzyl)phenoxy)acetate (**18a**).* Yellow oil (83% yield). ^{1}H NMR ($CDCl_3$): δ 1.27 (t, 3H, J = 7.1 Hz, CH_3), 4.02 (s, 2H, CH_2), 4.27 (q, 2H, J = 7.1 Hz, CH_2), 4.60 (s, 2H, CH_2), 6.86 (d, 2H, J = 8.4 Hz), 7.09 (d, 2H, J = 8.8 Hz), 7.31 (d, 2H, J = 8.8 Hz), 8.13 (d, 2H, J = 8.4 Hz) ppm. Anal. ($C_{17}H_{17}NO_5$) C, H, N % Calcd: 64.75 (C), 5.43 (H), 4.44 (N). % Found: 64.80 (C), 5.71 (H), 4.69 (N).

*Ethyl 2-(3-Methyl-4-(4-nitrobenzyl)phenoxy)acetate (**18b**).* Yellow oil (60% yield). ^{1}H NMR ($CDCl_3$): δ 1.26 (t, 3H, J = 7.0 Hz, CH_3), 2.12 (s, 3H, CH_3), 3.98 (s, 2H, CH_2), 4.23 (q, 2H, J = 7.0 Hz, CH_2), 4.57 (s, 2H, CH_2), 6.32−6.79 (m, 2H, Ar), 6.97 (d, 1H, J = 8.2 Hz, Ar), 7.21 (d, 2H, J = 8.5 Hz, Ar), 8.08 (d, 2H, J = 8.5 Hz, Ar) ppm. Anal. ($C_{18}H_{19}NO_5$) C, H, N % Calcd: 65.64 (C), 5.81 (H), 4.25 (N). % Found: 65.91 (C), 5.93 (H), 4.39 (N).

*2-(4-(4-Aminobenzyl)phenoxy)acetonitrile (**19a**).* A solution of **17a** (136 mg, 0.5 mmoli) in AcOH (10 mL) was hydrogenated in the presence of 10% Pd−C (28.3 mg), for 12 h. Then the catalyst was filtered off, and the solvent was removed to dryness to give a crude product that was used in the subsequent step without any further purification. Yellow oil. (52% yield). ^{1}H NMR ($CDCl_3$) δ: 3.83 (s, 2H, CH_2), 4.73 (s, 2H, CH_2CN), 6.63 (d, 2H, J = 8.4 Hz, Ar), 6.89 (d, 2H, J = 8.4 Hz, Ar), 6.95 (d, 2H, J = 8.4 Hz, Ar), 7.14 (d, 2H, J = 8.4 Hz, Ar) ppm. Anal. ($C_{15}H_{14}N_2O$) C, H, N % Calcd: 75.61 (C), 5.92 (H), 11.76 (N). % Found: 75.70 (C), 6.07 (H), 11.61 (N).

*2-(4-(4-Hydroxybenzyl)phenoxy)acetonitrile (**20a**).* To a mixture of aniline derivative **19a** (63.0 mg, 0.26 mmoli) in H_2O was added dropwise with H_2SO_{4conc} (0.06 mL) and the mixture was stirred at room temperature for 20 min. Then a solution of $NaNO_2$ (17.9 mg, 0.26 mmoli) in H_2O (0.19 mL) was added dropwise to the reaction mixture. The resulting solution was stirred for 1 h at 100 °C. The mixture was cooled to room temperature, and the residue diluted with AcOEt and washed with brine. The collected organic layers were dried and evaporated to give compound **20a** that was directly used in the next step. White solid; mp 151−153 °C (61% yield). ^{1}H NMR ($CDCl_3$) δ: 3.87 (s, 2H, CH_2), 4.74 (s, 2H, CH_2CN), 6.76 (d, 2H, J = 8.4 Hz, Ar), 6.90 (d, 2H, J = 8.4 Hz, Ar), 7.02 (d, 2H, J = 8.4 Hz, Ar), 7.14 (d, 2H, J = 8.4 Hz, Ar) ppm. Anal. ($C_{15}H_{13}NO_2$) C, H, N %

DOI: 10.1021/acs.jmedchem.5b00526
J. Med. Chem. 2015, 58, 5096−5107

Calcd: 75.30 (C), 5.48 (H), 5.85 (N). % Found: 74.92 (C), 5.48 (H), 6.13 (N).

Molecular Modeling. *mTAAR1 Homology Modeling.* In absence of crystallographic data for the TAAR1 receptor, we built a theoretical model of the *m*TAAR1, and then used it for docking simulations. Because most of the key residues characteristic of GPCRs are conserved in TAAR1 receptor, a *m*TAAR1 receptor homology model was generated, starting from the X-ray structure of human β_2-adrenoreceptor (PDB code 3PDS; resolution = 3.50 Å), in complex with an agonist compound.[35] The amino acid sequence of *m*TAAR1 (Q923Y8) was retrieved from the SWISSPROT database,[36] while the three-dimensional structure coordinates file of the GPCR template was obtained from the Protein Data Bank.[37]

The amino acid sequences of *m*TAAR1 TM helices were aligned with the corresponding residues of 3PDS, on the basis of the Blosum62 matrix (MOE software). The connecting loops were constructed by the loop search method implemented in MOE. The MOE output file included a series of ten *h*TAAR1 models which were independently built on the basis of a Boltzmann-weighted randomized procedure,[38] combined with specialized logic for the handling of sequence insertions and deletions.[39] Among the derived models, there were no significant main chain deviations. The model with the best packing quality function was selected for full energy minimization. The retained structure was minimized with MOE using the AMBER94 force field.[40] The energy minimization was carried out by the 1000 steps of steepest descent followed by conjugate gradient minimization until the rms gradient of the potential energy was less than 0.1 kcal mol^{-1} $Å^{-1}$. The assessment of the final obtained model was performed using Ramachandran plots, generated within MOE.

Following the same procedure already described by us,[34] the putative receptor model binding site was identified on the basis of the corresponding regions of the 3PDS binding site, and also by taking into account the recent mutagenesis data published by Grandy.[41]

Ligand Preparation. All compounds were built, parametrized (Gasteiger–Huckel method) and energy minimized within MOE using MMFF94 force field (MOE: Chemical Computing Group Inc., Montreal H3A2R7, Canada, http://www.chemcomp.comp). For all compounds, the protonated form was considered for the in silico analyses.

Docking Studies. Docking studies were subsequently performed, according to the following protocol. Each isomer was docked into the putative ligand binding site by means of the Surflex docking module implemented in Sybyl-X1.0. Then, for all the compounds, the best docking geometries (selected on the basis of the SurFlex scoring functions) were refined by ligand/receptor complex energy minimization (CHARMM27) by means of the MOE software. To verify the reliability of the derived docking poses, the obtained ligand/receptor complexes were further investigated by docking calculations (10 run), using MOE-Dock (Genetic algorithm; applied on the poses already located into the putative TAAR1 receptor). The conformers showing lower energy scoring functions and rmsd values (respect to the starting poses) were selected as the most stable and allowed us to identify the most probable conformers interacting with *m*TAAR1.

In Vitro Biological Studies. *Bioluminescence Resonance Energy Transfer (BRET) Measurement.* HEK-293 cells were transiently transfected with *m*TAAR1 and a cAMP BRET biosensor (EPAC) and then plated in a 96-well plate as described.[30] For time course experiments, the plate was read immediately after the addition of the agonist and for approximately 20 min. All the compounds were tested at the initial concentration of 10 μM. Then, for active compounds, a dose response was performed in order to calculate the EC_{50} values. All the experiments were conducted in the presence of the phosphodiesterase inhibitor IBMX (Sigma) at the final concentration of 200 μM. Readings were collected using a Tecan Infinite instrument that allows the sequential integration of the signals detected in the 465–505 nm and 515–555 nm windows using filters with the appropriate band-pass and by using iControl software. The acceptor/donor ratio was calculated as previously described.[42] Curve was fitted using a nonlinear regression and one site specific binding with GraphPad Prism 5. Data are representative of 4–6 independent experiments and are expressed as means ± SEM.

Cardiac Perfusion Technique. Male Wistar rats (275–300 g body wt), fed with standard diet, were anesthetized with a mixture of ether and air. After injection of 1000 U sodium heparin in the femoral vein, the heart was quickly excised and perfused according to the working heart technique, as described previously.[43] The height of the atrial and aortic cannulae was set at 20 and 100 cm, respectively. Unless otherwise specified, the perfusion buffer included (mM): 118 NaCl, 25 $NaHCO_3$, 4.5 KCl, 1.2 KH_2PO_4, 1.2 $MgSO_4$, 1.5 $CaCl_2$, and 11 glucose. Perfusions were carried out using 200 mL of recirculating buffer, which was equilibrated with a mixture of O_2 (95%) and CO_2 (5%). Temperature was kept between 36.8 and 37 °C, and the pH was 7.4.

After an equilibration period of 5 min, hearts were perfused for 60 min: 100 μL of DMSO (vehicle) or increasing doses of **2** and **3** dissolved in DMSO were added to the standard perfusion buffer. Aortic pressure and heart rate were continuously recorded on a personal computer. Cardiac output was determined as the sum of aortic and coronary flow. Powerlab/200 (ADInstruments, Castle Hill, Australia) was used for data acquisition.

Measurement of Plasma Glycaemia. Glycaemia was monitored in blood collected from the tail vein of 4 h (from 8 to 12 h) fasted mice (male, CD-1 strain), who had received T0AM, T1AM, **2**, and **3** (1.32, 4, and 11 $\mu g \cdot kg^{-1}$ ip) or saline (ip) (n = 10 in each group). Glycaemia was evaluated by a glucorefractometer 15 min after the ip injections, as described.[20] Data are expressed as mean ± SEM of independent experiments. Statistical analysis was performed by one-way ANOVA, followed by Student–Newman–Keuls multiple comparison post hoc test; the threshold of statistical significance was set at $P < 0.05$. Data analysis was performed by GraphPad Prism 5.0 statistical program (GraphPad software, San Diego, CA, USA).

■ ASSOCIATED CONTENT

Supporting Information

SMILES information on the compounds (CSV). The Supporting Information is available free of charge on the ACS Publications website at DOI: 10.1021/acs.jmedchem.5b00526.

■ AUTHOR INFORMATION

Corresponding Authors

*For G.C.: phone, +39 050 2218677; E-mail, g.chiellini@bm.med.unipi.it.

*For S.R.: phone, +39 050 2219582; E-mail, simona.rapposelli@farm.unipi.it.

Notes

The authors declare no competing financial interest.

■ ACKNOWLEDGMENTS

We thank Prof. Scanlan from the University of Oregon (USA) for supplying us T1AM, T0AM. This work was supported by a local grant from the University of Pisa (to G.C., R.Z., and S.R.). BRET studies has been supported by the Russian Science Foundation grant N14-25-00065 (to RRG).

■ ABBREVIATION USED

T1AM, 3-iodothyronamine; T0AM, thyronamine; β-PEA, β-phenylethylamine; TA0, thyroacetic acid; TA1, 3-iodothyroacetic acid

■ REFERENCES

(1) Scanlan, T. S.; Suchland, K. L.; Hart, M. E.; Chiellini, G.; Huang, Y.; Kruzich, P. J.; Frascarelli, S.; Crossley, D. A.; Bunzow, J. R.; Ronca-Testoni, S. 3-Iodothyronamine is an endogenous and rapid-acting derivative of thyroid hormone. *Nature Med.* **2004**, *10*, 638–642.

DOI: 10.1021/acs.jmedchem.5b00526
J. Med. Chem. 2015, 58, 5096–5107

(2) Saba, A.; Chiellini, G.; Frascarelli, S.; Marchini, M.; Ghelardoni, S.; Raffaelli, A.; Tonacchera, M.; Vitti, P.; Scanlan, T. S.; Zucchi, R. Tissue distribution and cardiac metabolism of 3-iodothyronamine. *Endocrinology* **2010**, *151*, 5063−5073.
(3) Hoefig, C. S.; Köhrle, J.; Brabant, G.; Dixit, K.; Yap, B.; Strasburger, C. J.; Wu, Z. Evidence for extrathyroidal formation of 3-iodothyronamine in humans as provided by a novel monoclonal antibody-based chemiluminescent serum immunoassay. *J. Clin. Endocrinol. Metab.* **2011**, *96*, 1864−1872.
(4) Hackenmueller, S. A.; Marchini, M.; Saba, A.; Zucchi, R.; Scanlan, T. S. Biosynthesis of 3-iodothyronamine (T1AM) is dependent on the sodium-iodide symporter and thyroperoxidase but does not involve extrathyroidal metabolism of T4. *Endocrinology* **2012**, *153*, 5659−5667.
(5) Höfig, C. W. T.; Lehmphul, I.; Daniel, H.; Schweizer, U.; Mittag, J.; Köhrle, J. Biosynthesis of 3-iodothyronamine from thyroxine in intestinal tissue. *Eur. Thyroid J.* **2014**, *3* (Suppl 1), 98−99.
(6) Revel, F.; Moreau, J.; Pouzet, B.; Mory, R.; Bradaia, A.; Buchy, D.; Metzler, V.; Chaboz, S.; Zbinden, K. G.; Galley, G. A new perspective for schizophrenia: TAAR1 agonists reveal antipsychotic-and antidepressant-like activity, improve cognition and control body weight. *Mol. Psychiatry* **2013**, *18*, 543−556.
(7) Espinoza, S.; Gainetdinov, R. R., Neuronal functions and emerging pharmacology of TAAR1. In *Topics in Medicinal Chemistry*; Springer: Berlin Heidelberg, Berlin, 2014; pp 1−20.
(8) Bunzow, J. R.; Sonders, M. S.; Arttamangkul, S.; Harrison, L. M.; Zhang, G.; Quigley, D. I.; Darland, T.; Suchland, K. L.; Pasumamula, S.; Kennedy, J. L. Amphetamine, 3,4-methylenedioxymethamphetamine, lysergic acid diethylamide, and metabolites of the catecholamine neurotransmitters are agonists of a rat trace amine receptor. *Mol. Pharmceutics* **2001**, *60*, 1181−1188.
(9) Borowsky, B.; Adham, N.; Jones, K. A.; Raddatz, R.; Artymyshyn, R.; Ogozalek, K. L.; Durkin, M. M.; Lakhlani, P. P.; Bonini, J. A.; Pathirana, S. Trace amines: identification of a family of mammalian G protein-coupled receptors. *Proc. Natl. Acad. Sci. U. S. A.* **2001**, *98*, 8966−8971.
(10) Lindemann, L.; Meyer, C. A.; Jeanneau, K.; Bradaia, A.; Ozmen, L.; Bluethmann, H.; Bettler, B.; Wettstein, J. G.; Borroni, E.; Moreau, J.-L. Trace amine-associated receptor 1 modulates dopaminergic activity. *J. Pharm. Exp. Ther.* **2008**, *324*, 948−956.
(11) Roy, G.; Placzek, E.; Scanlan, T. S. ApoB-100-containing Lipoproteins Are Major Carriers of 3-Iodothyronamine in Circulation. *J. Biol. Chem.* **2012**, *287*, 1790−1800.
(12) Dinter, J.; Mühlhaus, J.; Wienchol, C. L.; Yi, C.-X.; Nürnberg, D.; Morin, S.; Grüters, A.; Köhrle, J.; Schöneberg, T.; Tschöp, M. Inverse agonistic action of 3-iodothyronamine at the human trace amine-associated receptor 5. *PLoS One* **2015**, *10*, e0117774−e0117774.
(13) Chiellini, G.; Frascarelli, S.; Ghelardoni, S.; Carnicelli, V.; Tobias, S. C.; DeBarber, A.; Brogioni, S.; Ronca-Testoni, S.; Cerbai, E.; Grandy, D. K. Cardiac effects of 3-iodothyronamine: a new aminergic system modulating cardiac function. *FASEB J.* **2007**, *21*, 1597−1608.
(14) Ghelardoni, S.; Suffredini, S.; Frascarelli, S.; Brogioni, S.; Chiellini, G.; Ronca-Testoni, S.; Grandy, D. K.; Scanlan, T. S.; Cerbai, E.; Zucchi, R. Modulation of cardiac ionic homeostasis by 3-iodothyronamine. *J. Cell. Mol. Med.* **2009**, *13*, 3082−3090.
(15) Zucchi, R.; Accorroni, A.; Chiellini, G. Update on 3-iodothyronamine and its neurological and metabolic actions. *Front. Physiol.* **2014**, *5*, 402.
(16) Braulke, L.; Klingenspor, M.; DeBarber, A.; Tobias, S.; Grandy, D.; Scanlan, T.; Heldmaier, G. 3-Iodothyronamine: a novel hormone controlling the balance between glucose and lipid utilisation. *J. Comp. Physiol., B* **2008**, *178*, 167−177.
(17) Haviland, J.; Reiland, H.; Butz, D.; Tonelli, M.; Porter, W.; Zucchi, R.; Scanlan, T.; Chiellini, G.; Assadi-Porter, F. NMR-based metabolomics and breath studies show lipid and protein catabolism during low dose chronic T1AM treatment. *Obesity* **2013**, *21*, 2538−2544.
(18) Manni, M. E.; De Siena, G.; Saba, A.; Marchini, M.; Landucci, E.; Gerace, E.; Zazzeri, M.; Musilli, C.; Pellegrini-Giampietro, D.; Matucci, R. Pharmacological effects of 3-iodothyronamine (T1AM) in mice include facilitation of memory acquisition and retention and reduction of pain threshold. *Br. J. Pharmacol.* **2013**, *168*, 354−362.
(19) Klieverik, L. P.; Foppen, E.; Ackermans, M. T.; Serlie, M. J.; Sauerwein, H. P.; Scanlan, T. S.; Grandy, D. K.; Fliers, E.; Kalsbeek, A. Central effects of thyronamines on glucose metabolism in rats. *J. Endocrinol.* **2009**, *201*, 377−386.
(20) Manni, M. E.; De Siena, G.; Saba, A.; Marchini, M.; Dicembrini, I.; Bigagli, E.; Cinci, L.; Lodovici, M.; Chiellini, G.; Zucchi, R. 3-Iodothyronamine: a modulator of the hypothalamus−pancreas−thyroid axes in mice. *Br. J. Pharmacol.* **2012**, *166*, 650−658.
(21) Regard, J. B.; Kataoka, H.; Cano, D. A.; Camerer, E.; Yin, L.; Zheng, Y.-W.; Scanlan, T. S.; Hebrok, M.; Coughlin, S. R. Probing cell type-specific functions of Gi in vivo identifies GPCR regulators of insulin secretion. *J. Clin. Invest.* **2007**, *117*, 4034.
(22) Dhillo, W.; Bewick, G.; White, N.; Gardiner, J.; Thompson, E.; Bataveljic, A.; Murphy, K.; Roy, D.; Patel, N.; Scutt, J. The thyroid hormone derivative 3-iodothyronamine increases food intake in rodents. *Diabetes Obes. Metab.* **2009**, *11*, 251−260.
(23) Wood, W. J.; Geraci, T.; Nilsen, A.; DeBarber, A. E.; Scanlan, T. S. Iodothyronamines are oxidatively deaminated to iodothyroacetic acids in vivo. *ChemBioChem* **2009**, *10*, 361−365.
(24) Hackenmueller, S. A.; Scanlan, T. S. Identification and quantification of 3-iodothyronamine metabolites in mouse serum using liquid chromatography−tandem mass spectrometry. *J. Chromatogr., A* **2012**, *1256*, 89−97.
(25) Tan, E. S.; Groban, E. S.; Jacobson, M. P.; Scanlan, T. S. Toward deciphering the code to aminergic G protein-coupled receptor drug design. *Chem. Biol.* **2008**, *15*, 343−353.
(26) Hart, M. E.; Suchland, K. L.; Miyakawa, M.; Bunzow, J. R.; Grandy, D. K.; Scanlan, T. S. Trace amine-associated receptor agonists: synthesis and evaluation of thyronamines and related analogues. *J. Med. Chem.* **2006**, *49*, 1101−1112.
(27) Chiellini, G.; Apriletti, J. W.; Al Yoshihara, H.; Baxter, J. D.; Ribeiro, R. C.; Scanlan, T. S. A high-affinity subtype-selective agonist ligand for the thyroid hormone receptor. *Chem. Biol.* **1998**, *5*, 299−306.
(28) Molander, G. A.; Elia, M. D. Suzuki−Miyaura cross-coupling reactions of benzyl halides with potassium aryltrifluoroborates. *J. Org. Chem.* **2006**, *71*, 9198−9202.
(29) Barak, L. S.; Salahpour, A.; Zhang, X.; Masri, B.; Sotnikova, T. D.; Ramsey, A. J.; Violin, J. D.; Lefkowitz, R. J.; Caron, M. G.; Gainetdinov, R. R. Pharmacological characterization of membrane-expressed human trace amine-associated receptor 1 (TAAR1) by a bioluminescence resonance energy transfer cAMP biosensor. *Mol. Pharmacol.* **2008**, *74*, 585−594.
(30) Espinoza, S.; Salahpour, A.; Masri, B.; Sotnikova, T. D.; Messa, M.; Barak, L. S.; Caron, M. G.; Gainetdinov, R. R. Functional interaction between trace amine-associated receptor 1 and dopamine D2 receptor. *Mol. Pharmacol.* **2011**, *80*, 416−25.
(31) Ghelardoni, S.; Chiellini, G.; Frascarelli, S.; Saba, A.; Zucchi, R. Uptake and metabolic effects of 3-iodothyronamine in hepatocytes. *J. Endocrinol.* **2014**, *221*, 101−110.
(32) Moro, S.; Deflorian, F.; Bacilieri, M.; Spalluto, G. Ligand-based homology modeling as attractive tool to inspect GPCR structural plasticity. *Curr. Pharm. Des.* **2006**, *12*, 2175−2185.
(33) Cichero, E.; Espinoza, S.; Gainetdinov, R. R.; Brasili, L.; Fossa, P. Insights into the structure and pharmacology of the human trace amine-associated receptor 1 (hTAAR1): homology modelling and docking studies. *Chem. Biol. Drug Des.* **2013**, *81*, 509−516.
(34) Cichero, E.; D'Ursi, P.; Moscatelli, M.; Bruno, O.; Orro, A.; Rotolo, C.; Milanesi, L.; Fossa, P. Homology modeling, docking studies and molecular dynamic simulations using graphical processing unit architecture to probe the type-11 phosphodiesterase catalytic site: a computational approach for the rational design of selective inhibitors. *Chem. Biol. Drug Des.* **2013**, *82*, 718−731.

DOI: 10.1021/acs.jmedchem.5b00526
J. Med. Chem. 2015, 58, 5096−5107

(35) Rosenbaum, D. M.; Zhang, C.; Lyons, J. A.; Holl, R.; Aragao, D.; Arlow, D. H.; Rasmussen, S. G.; Choi, H.-J.; DeVree, B. T.; Sunahara, R. K. Structure and function of an irreversible agonist-β2 adrenoceptor complex. *Nature* **2011**, *469*, 236−240.
(36) Bairoch, A.; Apweiler, R. The SWISS-PROT protein sequence database and its supplement TrEMBL in 2000. *Nucleic Acids Res.* **2000**, *28*, 45−48.
(37) Berman, H. M.; Westbrook, J.; Feng, Z.; Gilliland, G.; Bhat, T.; Weissig, H.; Shindyalov, I. N.; Bourne, P. E. The Protein Data Bank. *Nucleic Acids Res.* **2000**, *28*, 235−242.
(38) Levitt, M. Accurate modeling of protein conformation by automatic segment matching. *J. Mol. Biol.* **1992**, *226*, 507−533.
(39) Fechteler, T.; Dengler, U.; Schomburg, D. Prediction of protein three-dimensional structures in insertion and deletion regions: a procedure for searching data bases of representative protein fragments using geometric scoring criteria. *J. Mol. Biol.* **1995**, *253*, 114−131.
(40) Cornell, W. D.; Cieplak, P.; Bayly, C. I.; Gould, I. R.; Merz, K. M.; Ferguson, D. M.; Spellmeyer, D. C.; Fox, T.; Caldwell, J. W.; Kollman, P. A. A second generation force field for the simulation of proteins, nucleic acids, and organic molecules. *J. Am. Chem. Soc.* **1996**, *118*, 2309−2309.
(41) Reese, E. A.; Norimatsu, Y.; Grandy, M. S.; Suchland, K. L.; Bunzow, J. R.; Grandy, D. K. Exploring the determinants of trace amine-associated receptor 1's functional selectivity for the stereoisomers of amphetamine and methamphetamine. *J. Med. Chem.* **2014**, *5*, 378−390.
(42) Salahpour, A.; Espinoza, S.; Masri, B.; Lam, V.; Barak, L. S.; Gainetdinov, R. R. BRET biosensors to study GPCR biology, pharmacology, and signal transduction. *Front. Endocrinol.* **2012**, *3*, 105.
(43) Zucchi, R.; Ronca-Testoni, S.; Yu, G.; Galbani, P.; Ronca, G.; Mariani, M. Effect of ischemia and reperfusion on cardiac ryanodine receptors-sarcoplasmic reticulum Ca^{2+} channels. *Circ. Res.* **1994**, *74*, 271−280.

DOI: 10.1021/acs.jmedchem.5b00526
J. Med. Chem. 2015, 58, 5096−5107